京都大学学術情報リポジトリ
KURENAI 紅
Kyoto University Research Information Repository

京都大学
KYOTO UNIVERSITY

Title	Sliding-Mode Control for Transformation to an Inverted Pendulum Mode of a Mobile Robot With Wheel-Arms
Author(s)	Fukushima, Hiroaki; Muro, Keiji; Matsuno, Fumitoshi
Citation	IEEE Transactions on Industrial Electronics (2015), 62(7): 4257-4266
Issue Date	2015-07
URL	http://hdl.handle.net/2433/200677
Right	© 2014 IEEE. Personal use of this material is permitted. Permission from IEEE must be obtained for all other uses, in any current or future media, including reprinting/republishing this material for advertising or promotional purposes, creating new collective works, for resale or redistribution to servers or lists, or reuse of any copyrighted component of this work in other works.
Type	Journal Article
Textversion	author

Kyoto University

Sliding Mode Control for Transformation to an Inverted Pendulum Mode of a Mobile Robot with Wheel-Arms

Hiroaki Fukushima, *Member, IEEE*, Keiji Muro, and Fumitoshi Matsuno, *Member, IEEE*

***Abstract*—This paper proposes a control method for locomotion mode transformation of a mobile robot with wheel-arms. The proposed method aims at transformation from a four-wheeled mode for high speed mobility to an inverted pendulum mode, which has advantages of high viewing position and small turning radius. Since the initial state of the system is far away from the target equilibrium point of the wheeled inverted pendulum system, we use a nonlinear controller based on sliding mode control. In contrast that the previous transformation methods cannot control the robot velocity until the robot body is lifted up, the proposed method can take into account the robot velocity from the beginning of the transformation, which enables to complete the transformation in a smaller space. To analyze the asymptotic stability of the control system on the sliding surface, we derive an invariant set in which the system state converges to the origin without going out. Furthermore, the effectiveness of the proposed method is demonstrated in both simulations and real robot experiments.**

***Index Terms*—Wheeled inverted pendulum, locomotion mode transformation, sliding mode control, invariant set.**

I. Introduction

WHEELED mobile robots often face more difficulties when traversing rough terrain compared with tracked or legged robots, in contrast to the high mobility on flat floors. For this reason, modifications on wheeled robots have been made to allow them to conquer complex environments, such as the switching mechanism between a wheel and a track [1] and the wheeled-legged robots [2]–[6].

For the same purpose, another type of wheeled robot was proposed in [7]. As shown in Fig. 1, this robot has arms (or flippers) equipped with wheels, which we call "wheel-arms", on both sides of the main body equipped with a camera on the top. By using the arms, the robot can climb over obstacles [8]. This robot has two inverted pendulum modes, which enable to turn in confined space and provide high viewing position [9]–[10]. Another remarkable feature of this robot is that the high mobility on flat floors of ordinary wheeled robots is maintained, since the four wheeled mode has a similar form to ordinary wheeled robots.

Manuscript received March 27, 2014; revised July 8, 2014, September 1, 2014 and October 18, 2014; accepted November 20, 2014.

Copyright © 2014 IEEE. Personal use of this material is permitted. However, permission to use this material for any other purposes must be obtained from the IEEE by sending a request to pubs-permissions@ieee.org.

H. Fukushima, K. Muro, and F. Matsuno are with the Department of Mechanical Engineering and Science, Kyoto University, Kyoto, Japan (e-mail: fuku@me.kyoto-u.ac.jp; sml66keg@gmail.com; matsuno@me.kyoto-u.ac.jp)

In the same way as in [9]–[10], this paper focuses on transformation from a four wheeled mode to an inverted pendulum mode, as illustrated in Fig. 2. The transformation starts with lifting up the wheel-arms to raise the center of gravity (COG) of the whole robot (**2** of Fig. 2), due to the motor torque limits. Then, the robot body is lifted up, while returning the arms to the initial angle. A problem of the control methods in [9]–[10] is that the velocity of the robot is not controlled until the body pitch angle and the arm angle are controlled to the target values, as in **4** of Fig. 2. As a result, a considerable amount of space is required before the robot completes the transformation and stops. This problem is mainly caused by the underactuation and the complexity of the system.

A. Related Work

Control system design for wheeled inverted pendulums has been intensively studied in the literature. Many of early studies adopt linear controllers [11]–[16] based on a linear approximation of a nonlinear model around an equilibrium point. A limitation of linear controllers is that they are not necessarily effective in cases where the system state is far from the equilibrium point, such as in our transformation problem.

More recent studies have proposed various nonlinear control methods for wheeled inverted pendulums [17]–[37]. They can be classified by how to deal with the underactuation, which occurs mainly because both the velocity (or position) of the vehicle and the pitch angle of the body need to be controlled by a single actuator.

A common approach to deal with the underactuation is the "two-level" control [17]–[23]. In this approach, the pitch angle of the body is controlled to a given target angle by an actuator, while the velocity (or position) of the vehicle is controlled by

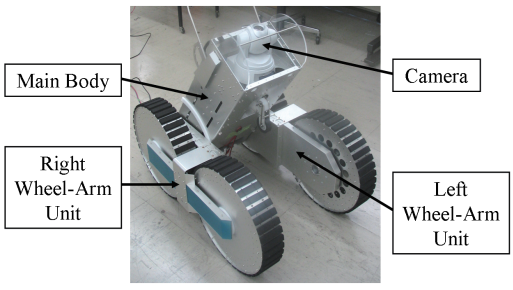

Fig. 1. Mobile robot with wheel-arms.

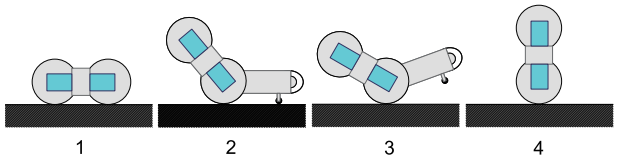

Fig. 2. Schematic of transformation.

manipulating the target pitch angle of the body. The two-level control methods can be further classified by how to determine the target pitch angle of the body.

In [17]–[20], the control design of the velocity and its convergence analysis are enabled by simplifying the system model based on two strong assumptions that the body angle perfectly tracks the target value and that the body angular velocity is negligible. In order to make these assumptions easier to be satisfied, [18] proposed a method based on model predictive control (see e.g. [24]–[26]), which aims to limit the frequency band of reference signals for the body angle. However, there is still no guarantee that the assumptions mentioned above are satisfied. Further, the implementation of this method is difficult, since a nonlinear optimization problem needs to be solved in real time.

On the other hand, [9]–[10] use a more relaxed assumption that tracking errors of the body angle and body angular velocity from constant target values are negligible after a given period of time. However, since the initial body and arm angles are assumed to be zero in the velocity control methods in [9]–[10], they cannot be applied from the beginning of the transformation process, as mentioned earlier.

In [21]–[22], the target body angle, which is changed for position control, is simply chosen by a linear function of the position error. While these studies investigate the convergence of the body angle and tuning parameters of an adaptive controller, no theoretical result is presented on the convergence of the vehicle position.

A neural network is used in [23] to approximate a system that generates a reference signal of the body angle such that the vehicle position and velocity converge to target values. An ultimate bound of the tracking errors of the vehicle position and velocity is derived without one of the strong assumptions, mentioned above, that the body angular velocity is negligible. However, it is difficult to know how small this error bound is, since the bound is described by using a parameter whose value is difficult to estimate. The same problem arises in [27]–[30], where the error bound is expected to be larger than the one in [23], since the controllers in [27]–[30] do not have the feedback loop for the vehicle velocity and position.

Another approach to deal with the underactuation is to choose controlled variables such that the internal dynamics is asymptotically stable when the controlled variables are kept to zero. Sliding mode control methods in [31]–[32] choose a controlled variable as a function of the body angle, the body angular velocity, and the vehicle velocity. In addition to the convergence of the controlled variable, the asymptotic stability on the sliding surface, on which the controlled variable is zero, is discussed based on the linear approximation of the system. A limitation of the stability analysis based on the linear approximation is that the region of attraction of the target equilibrium point is not clarified, even if it can be ensured that the target equilibrium point is asymptotically stable.

Other methods using fuzzy control [33]–[36] and neural network with PID control [37] have also been proposed. Since these methods use an approximation model of the original dynamic model of an wheeled inverted pendulum or do not use any model, the convergence analysis for the original dynamic model is difficult.

Transformation from a four-wheeled vehicle to an inverted pendulum has also been studied for other types of robots. In [38], the transformation is achieved using two-link arms, which have a roller at the end of each arm. Since this robot can lift up the COG to the neighborhood of the equilibrium point by using the arms, a linear controller is used to control the body angle. The robot in [39], [40] also achieves the transformation from a four-wheeled vehicle to an inverted pendulum. Unlike other inverted pendulum type wheeled robots, the balance control is achieved by adjusting joint angles of arms or the body. We do not consider situations where this kind of balance control is applicable, since it is difficult for many other robots including the one which this paper focuses on.

In contrast that some of the studies mentioned above consider model uncertainties [20], [22], [27]–[29], [31], [32] and movement on inclined planes [19], [31], [32], [36], we do not take into account them in the control system design. Instead, we focus on the fact that convergence analysis of both the body angle and the vehicle velocity of the wheeled inverted pendulum is still a challenging issue even under the assumption of no model uncertainty and no inclined plane, due to the underactuation and the complexity of the system.

B. Contribution of This Paper

This paper proposes a sliding mode control method for transformation to an inverted pendulum mode of a mobile robot with wheel-arms. In contrast to the previous transformation methods based on the two-level control [9]–[10], the proposed method can take into account the robot velocity from the beginning of the transformation, which enables to complete the transformation in a smaller space. Furthermore, unlike the sliding mode control method for mobile inverted pendulums [31]–[32], the region of attraction on the sliding surface is clarified by deriving an invariant set in which the system state converges to the origin without going out. The effectiveness of the proposed method is demonstrated in both simulations and real robot experiments.

II. Control Objective

As mentioned in Section I, we focus on the transformation from the four wheeled mode to the inverted pendulum mode, as illustrated in Fig. 2. More precisely, this paper proposes a control algorithm for transformation from **2** to **4**, since the transformation from **1** to **2** can be easily achieved. Therefore,

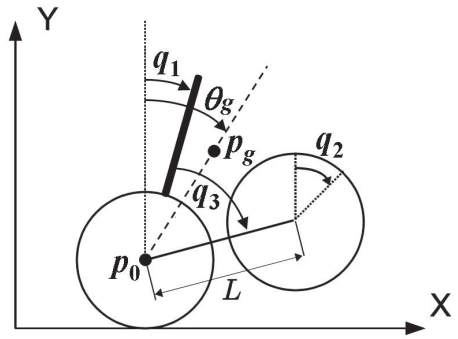

Fig. 3. Schematic of parameters.

we first describe the dynamic model of the robot in the transformation from **2** to **4**.

As illustrated in Fig. 3, q_1 denotes the angle of the main body with respect to the vertical direction, q_2 is the rotation angle of the wheels, and q_3 is the relative angle of the arms with respective to the main body. Let u_1 and u_2 denote the motor current values to control each arm and wheel, respectively. The definition of other parameters are shown in Table I. We assume that the left and right wheel angles are always the same as each other, since the same input command is given to the left and right motors. Also, q_3 is assumed to take the same value for both left and right arms, since the same reference trajectory is always given for both arms. Under these assumptions, the motion of the robot is restricted to the $X-Y$ plane in Fig. 3. The equations of motion can be derived using Lagrange's equations, as follows:

$$M(q)\ddot{q} + C(q,\dot{q}) + G(q) = Eu, \tag{1}$$

where $q = [q_1, q_2, q_3]^T$, $u = [u_1, u_2]^T$, and the elements of $M(q) \in \mathbb{R}^{3\times3}$, $C(q,\dot{q}) \in \mathbb{R}^3$, $G(q) \in \mathbb{R}^3$, $E \in \mathbb{R}^{3\times2}$ are described as

$$\begin{aligned}
M_{11} &= m_1 l_1^2 + 2m_3 l_2^2 + 2m_4 L^2 + J_1 + 2J_3 \\
M_{12} &= M_{21} = r\{\beta_1 \cos q_1 + 2\beta_2 \cos(q_1 + q_3)\} \\
M_{13} &= M_{31} = M_{33} = 2m_3 l_2^2 + 2J_3 + 2m_4 L^2 \\
M_{22} &= (m_1 + 2m_3 + 2m_4 + 2m_2) r^2 + 2J_4 + 2J_2 \\
M_{23} &= M_{32} = 2\beta_2 r \cos(q_1 + q_3) \\
C_1 &= C_3 = G_2 = E_{21} = 0 \\
C_2 &= -r\{\beta_1 \dot{q}_1^2 \sin q_1 + 2\beta_2 (\dot{q}_1 + \dot{q}_3)^2 \sin(q_1 + q_3)\} \\
G_1 &= -\beta_1 g \sin q_1 - 2\beta_2 g \sin(q_1 + q_3) \\
G_3 &= -2\beta_2 g \sin(q_1 + q_3) \\
E_{11} &= -E_{31} = -2n_1 K_{t1} \\
E_{12} &= E_{32} = -E_{22} = -2n_2 K_{t2}
\end{aligned}$$

where $\beta_1 := m_1 l_1$, $\beta_2 := m_3 l_2 + m_4 L$ and g is the acceleration of gravity. Furthermore, (1) can be rewritten as

$$\begin{aligned}
&\ddot{q} = \bar{f}(q,\dot{q}) + \bar{g}(q)u \qquad (2)\\
&\bar{f}(q,\dot{q}) := M(q)^{-1}\big(-C(q,\dot{q}) - G(q)\big),\ \bar{g}(q) := M(q)^{-1}E.
\end{aligned}$$

Our goal is to steer (q_1, q_3, $\dot{q}_2$) from the initial state ($\pi/2$, $q_3(0)$, 0) as in **2** of Fig. 2 to (0, 0, 0) as in **4** of Fig. 2 for some $q_3(0) \neq 0$. However, when $q_3 \neq 0$, the robot as a whole is not balanced even if $q_1 = 0$. Thus, the angle of the whole body θ_g, described below, is controlled instead of directly controlling q_1. If θ_g and q_3 are controlled to 0, then q_1 is also controlled to 0, indirectly. As shown in Fig. 3, θ_g is the angle measured clockwise from the vertical direction to the vector from p_0 to p_g, where p_0 and p_g are the center of the rear wheels and the COG of the robot, respectively. By "the rear wheels", we mean the wheels attached to the main body (the one on the ground in Fig. 3), whereas "the front wheels" are the other wheels attached at the end of the arms. More precisely, θ_g is described as

$$\theta_g = q_1 + \alpha \tag{3}$$

$$\alpha := \tan^{-1} \frac{2\beta_2 \sin q_3}{\beta_1 + 2\beta_2 \cos q_3}. \tag{4}$$

Thus, $\dot{\theta}_g$ is obtained as

$$\dot{\theta}_g = \dot{q}_1 + \dot{\alpha} = \dot{q}_1 + \zeta(q_3)\dot{q}_3 \tag{5}$$

$$\zeta(q_3) := \frac{4\beta_2^2 + 2\beta_1\beta_2 \cos q_3}{\beta_1^2 + 4\beta_2^2 + 4\beta_1\beta_2 \cos q_3}. \tag{6}$$

See [10] for the details on the model including the values of physical parameters and on the derivation of θ_g.

TABLE I
DEFINITION OF PARAMETERS.

m_1	Mass of main body	J_1	Moment of inertia of main body
m_2	Mass of rear wheel	J_2	Moment of inertia of rear wheel
m_3	Mass of arm	J_3	Moment of inertia of arm
m_4	Mass of front wheel	J_4	Moment of inertia of front wheel
r	Radius of wheel	l_1	Length to COG of main body
L	Length of arm	l_2	Length to COG of arm
n_1	Arm motor gear ratio	K_{t1}	Arm motor torque constant
n_2	Wheel motor gear ratio	K_{t2}	Wheel motor torque constant

III. SLIDING MODE CONTROLLER DESIGN

We use the sliding surface $s = 0$ for the following s:

$$s = \begin{bmatrix} s_1 \\ s_2 \end{bmatrix} = \begin{bmatrix} \lambda_1\theta_g + \lambda_2\dot{\theta}_g + \dot{q}_2 \\ \lambda_3 q_3 + \dot{q}_3 \end{bmatrix} \tag{7}$$

where λ_i ($i = 1, 2, 3$) is a constant number determined by a designer. It follows from (2) that

$$\begin{aligned}
\ddot{q}_1 &= \bar{f}_1 + \bar{g}_{11}u_1 + \bar{g}_{12}u_2 \\
\ddot{q}_2 &= \bar{f}_2 + \bar{g}_{21}u_1 + \bar{g}_{22}u_2 \\
\ddot{q}_3 &= \bar{f}_3 + \bar{g}_{31}u_1 + \bar{g}_{32}u_2.
\end{aligned} \tag{8}$$

where $\bar{f}_i$ ($i = 1, 2, 3$) is the ith element of $\bar{f}$, and $\bar{g}_{ij}$ ($i = 1, 2, 3$, $j = 1, 2$) is the (i, j) element of $\bar{g}$. By differentiating (5), we obtain

$$\ddot{\theta}_g = \ddot{q}_1 + \frac{\partial\zeta}{\partial q_3}\dot{q}_3^2 + \zeta\ddot{q}_3. \tag{9}$$

Thus, it holds from (7) and (8)–(9) that

$$\dot{s} = A + Bu \tag{10}$$

where

$$A := \begin{bmatrix} \lambda_1\dot{\theta}_g + \lambda_2\left(\bar{f}_1 + \dfrac{\partial\zeta}{\partial q_3}\dot{q}_3^2 + \zeta\bar{f}_3\right) + \bar{f}_2 \\ \lambda_3\dot{q}_3 + \bar{f}_3 \end{bmatrix}$$
$$B := \begin{bmatrix} \lambda_2(\bar{g}_{11} + \zeta\bar{g}_{31}) + \bar{g}_{21} & \lambda_2(\bar{g}_{12} + \zeta\bar{g}_{32}) + \bar{g}_{22} \\ \bar{g}_{31} & \bar{g}_{32} \end{bmatrix}.$$

By following a standard way for multi-input sliding mode control [41], the feedback law is decided as

$$u = -B^{-1}(A + K\mathrm{sgn}(s)) \tag{11}$$

where sgn(s) denotes the vector of the signum functions of each element of s, and $K = \mathrm{diag}(k_1, k_2)$ for positive constants k_1 and k_2. By substituting (11) into (10), we obtain

$$\dot{s}_1 = -k_1\mathrm{sgn}(s_1), \quad \dot{s}_2 = -k_2\mathrm{sgn}(s_2). \tag{12}$$

Thus, $s_1(t)$ and $s_2(t)$ reach zero, and they remain to be zero once they reach zero. On the nonsingularity of B, we have the following property.

Proposition 1: If λ_2 is chosen such that $\lambda_2 \geq 2$ and $2\lambda_2 M_{22} - M_{11} - M_{13} > 0$, then B is nonsingular.

Proof: The determinant of B is described as

$$\det(B) = E_1E_2\{2\lambda_2M_{22} - M_{11} - M_{13} + \lambda_2M_{23} + (\lambda_2 - 2)M_{12}\}/\det(M), \tag{13}$$

where $E_1 := 2n_1K_{t1}$ and $E_2 := 2n_2K_{t2}$. Since $|q_1| \leq \pi/2$ and $|q_1 + q_3| \leq \pi/2$ are always satisfied, we have $M_{12} \geq 0$ and $M_{23} \geq 0$. Thus, it holds from the assumptions that $2\lambda_2M_{22} - M_{11} - M_{13} + \lambda_2M_{23} + (\lambda_2 - 2)M_{12} > 0$. Therefore, since $E_1 > 0$, $E_2 > 0$, and $\det(M)$ is bounded, it is proved that $\det(B) \neq 0$. ∎

IV. Stability Analysis on the Sliding Surface

Since $s(t)$ is maintained as zero as shown in Section III, we now analyze the behavior of the system on the sliding surface $s = 0$. From the definition of s in (7), the following constraints are satisfied on the sliding surface

$$s_1 = \lambda_1\theta_g + \lambda_2\dot{\theta}_g + \dot{q}_2 = 0 \tag{14}$$
$$s_2 = \lambda_3q_3 + \dot{q}_3 = 0. \tag{15}$$

From (15), it is easily seen that q_3 converges to zero on the sliding surface, if $\lambda_3 > 0$. Therefore, we next analyze the behavior of $(\theta_g, \dot{\theta}_g, \dot{q}_2)$, when $s_1 = 0$ and $q_3 = 0$. More precisely, we analyze the convergence of $(\theta_g, \dot{\theta}_g)$, since (14) implies that $\dot{q}_2$ converges to zero if $(\theta_g, \dot{\theta}_g)$ converges to zero.

To this end, we first describe the system model for $s_1 = 0$ and $q_3 = 0$. Since (1) implies

$$M_{11}\ddot{q}_1 + M_{12}\ddot{q}_2 + M_{13}\ddot{q}_3 + G_1 = -2n_1K_{t1}u_1 - 2n_2K_{t2}u_2$$
$$M_{21}\ddot{q}_1 + M_{22}\ddot{q}_2 + M_{23}\ddot{q}_3 + C_2 = 2n_2K_{t2}u_2$$
$$M_{31}\ddot{q}_1 + M_{32}\ddot{q}_2 + M_{33}\ddot{q}_3 + G_3 = 2n_1K_{t1}u_1 - 2n_2K_{t2}u_2,$$

we obtain the following relationship without u_1 and u_2

$$N_1\ddot{q}_1 + N_2\ddot{q}_2 + N_3\ddot{q}_3 + N_4 = 0 \tag{16}$$

where $N_1 := M_{11} + 2M_{21} + M_{31}$, $N_2 := M_{12} + 2M_{22} + M_{32}$, $N_3 := M_{13} + 2M_{23} + M_{33}$, $N_4 := G_1 + 2C_2 + G_3$. We also obtain

$$\ddot{q}_2 = -\lambda_1\dot{\theta}_g - \lambda_2\ddot{\theta}_g \tag{17}$$

by differentiating (14). Since $q_1 = \theta_g$ for $q_3 = 0$, it holds from (16)–(17) and $q_3 = 0$ that

$$\ddot{\theta}_g = -F_1\dot{\theta}_g - F_2\sin\theta_g \tag{18}$$

where

$$F_1 := \frac{a_1 + a_2\cos\theta_g}{d_1 + d_2\cos\theta_g}, \quad F_2 := \frac{b_1 + b_2\dot{\theta}_g^2}{d_1 + d_2\cos\theta_g} \tag{19}$$
$$a_1 := 2M_{22}\lambda_1, \quad a_2 := (\beta_1 + 4\beta_2)r\lambda_1 \tag{20}$$
$$b_1 := (\beta_1 + 4\beta_2)g, \quad b_2 := 2(\beta_1 + 2\beta_2)r$$
$$d_1 := 2M_{22}\lambda_2 - M_{11} - M_{31}$$
$$d_2 := \{(\beta_1 + 4\beta_2)\lambda_2 - 2(\beta_1 + 2\beta_2)\}r.$$

To analyze the convergence of $(\theta_g, \dot{\theta}_g)$, we consider a region $\mathcal{E}$ of $x_\theta := [\theta_g, \dot{\theta}_g]^T$ as follows

$$\mathcal{E} := \{x_\theta |\ V(x_\theta) \leq \gamma\} \tag{21}$$
$$V(x_\theta) = x_\theta^T P x_\theta, \quad P = \begin{bmatrix} p_{11} & p_{12} \\ p_{12} & p_{22} \end{bmatrix}, \tag{22}$$

where P is a constant positive definite matrix, and γ is a positive constant. If $\dot{V} < 0$ is satisfied for $x_\theta \neq 0$ in $\mathcal{E}$, x_θ converges to 0 without going out of the set, once x_θ is in $\mathcal{E}$. Before we derive the conditions of P, γ and λ_i $(i = 1, 2)$ to guarantee $\dot{V} < 0$ in $\mathcal{E}$, we define the following.

$$\bar{F}_1 := \max\left\{\frac{a_1 + a_2}{d_1 + d_2}, \frac{a_1}{d_1}\right\}, \ \underline{F}_1 := \min\left\{\frac{a_1 + a_2}{d_1 + d_2}, \frac{a_1}{d_1}\right\}$$
$$\bar{h}_1 := \frac{(p_{12}\bar{F}_1 + p_{11})p_{22} - 2p_{12}^2}{p_{22}^2}, \quad \underline{F}_2 := \frac{b_1}{d_1 + d_2}$$
$$\underline{h}_1 := \frac{(p_{12}\underline{F}_1 + p_{11})p_{22} - 2p_{12}^2}{p_{22}^2}$$
$$\underline{h}_2 := p_{22}^2\underline{h}_1^2 - (p_{11} - p_{12}\underline{F}_1)^2, \quad S := \frac{\sqrt{\underline{h}_2}}{p_{22}} + \underline{h}_1$$

Now the condition for P and λ_i is described as follows.

Assumption 1: The following inequalities are satisfied.

$$d_1 > 0, \quad d_2 > 0, \quad \underline{h}_2 > 0, \quad \underline{h}_1 > 0 \tag{23}$$
$$p_{12} > 0, \quad p_{11} - p_{12}\bar{F}_1 > 0 \tag{24}$$
$$p_{22}\left(\frac{2}{\pi}\underline{F}_2 - \bar{h}_1\right) + \sqrt{\underline{h}_2} > 0 \tag{25}$$
$$S(d_1 + d_2) - b_1 > 0 \tag{26}$$

Note that all the conditions in Assumption 1 can be checked using known values of the physical parameters of the system and design parameters P, λ_1 and λ_2. Based on the assumption above, we obtain the following result.

Theorem 1: Under Assumption 1, $\dot{V} < 0$ is satisfied for $x_\theta \neq 0$ in $\mathcal{E}$, if γ is the minimum eigenvalue of $P^{\frac{1}{2}}U^{-1}P^{\frac{1}{2}}$ where $U := \mathrm{diag}(U_1, U_2)$ for

$$U_1 := \frac{Sd_2}{2\{S(d_1 + d_2) - b_1\}}, \quad U_2 := \frac{b_2}{S(d_1 + d_2) - b_1}.$$

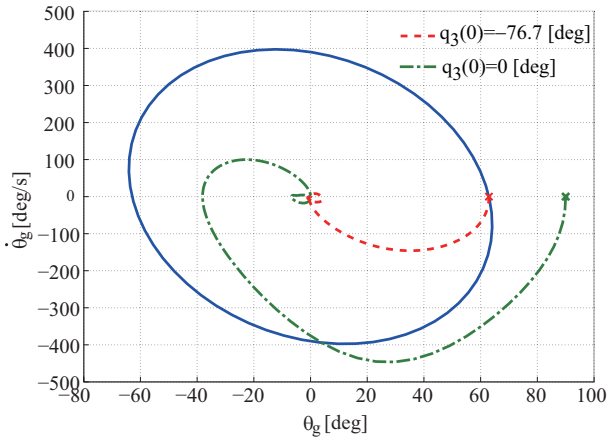

Fig. 4. Invariant set of x_θ for $s_1 = 0$ and $q_3 = 0$.

Proof: See Appendix. ■

Based on Theorem 1 above, the values of λ_1, λ_2 and P should be chosen such that Assumption 1 is satisfied for as large γ as possible, in order to obtain a large region of attraction $\mathcal{E}$. On the other hand, k_1, k_2 and λ_3 can be chosen irrespective to Theorem 1. By choosing large values of k_1, k_2 and λ_3, the trajectory of the state rapidly goes to the surface of $s_1 = q_3 = 0$, although the values are limited due to the motor torque limitation of the real robot. Unfortunately, since no other guideline is currently available, the values of the parameters need to be selected by trial and error.

Since s_1 and q_3 go to 0 by using our controller, the stability for $s_1 = q_3 = 0$ is a fundamental property required for the closed-loop system. However, it should be noted that the stability for $s_1 \neq 0, q_3 \neq 0$ is not proved, even if $(\theta_g, \dot{\theta}_g)$ is in $\mathcal{E}$ at the initial time. The possibility that $(\theta_g, \dot{\theta}_g)$ goes out of $\mathcal{E}$ by decreasing s_1 cannot be denied theoretically, although such a behavior is not seen in our simulations. We leave the stability analysis for $s_1 \neq 0, q_3 \neq 0$ as a future work.

V. Simulation

The design parameters in (7) and (11) are chosen as

$$\lambda_1 = 4, \quad \lambda_2 = 2, \quad \lambda_3 = 1, \quad K = \mathrm{diag}(2, 2).$$

The value of λ_2 above satisfies the condition for nonsingularity of B in Proposition 1. Fig. 4 shows the region $\mathcal{E}$ in Theorem 1 when P is chosen as

$$P = R^T \begin{bmatrix} 40 & 0 \\ 0 & 1 \end{bmatrix} R, \quad R = \begin{bmatrix} \cos\frac{\pi}{100} & -\sin\frac{\pi}{100} \\ \sin\frac{\pi}{100} & \cos\frac{\pi}{100} \end{bmatrix}.$$

The initial state of the simulation is illustrated in **2** of Fig. 2. By performing simulations for various values of the initial arm angle $q_3(0)$ from -180 [deg] to 0 [deg] with the resolution of 0.1 [deg], we confirmed that the trajectories of $(\theta_g, \dot{\theta}_g)$ do not go out of $\mathcal{E}$ once the trajectories go into $\mathcal{E}$, which is not theoretically proved for $s_1 \neq 0$ and $q_3 \neq 0$. The trajectories of $(\theta_g, \dot{\theta}_g)$ from the initial state on the boundary of $\mathcal{E}$ ($q_3 = -76.7$) and the initial state with the maximum θ_g ($q_3 = 0$) are shown in dashed and dash-dotted lines respectively in Fig. 4, as examples. The marks "×" in Fig. 4 denote the initial states of the trajectories.

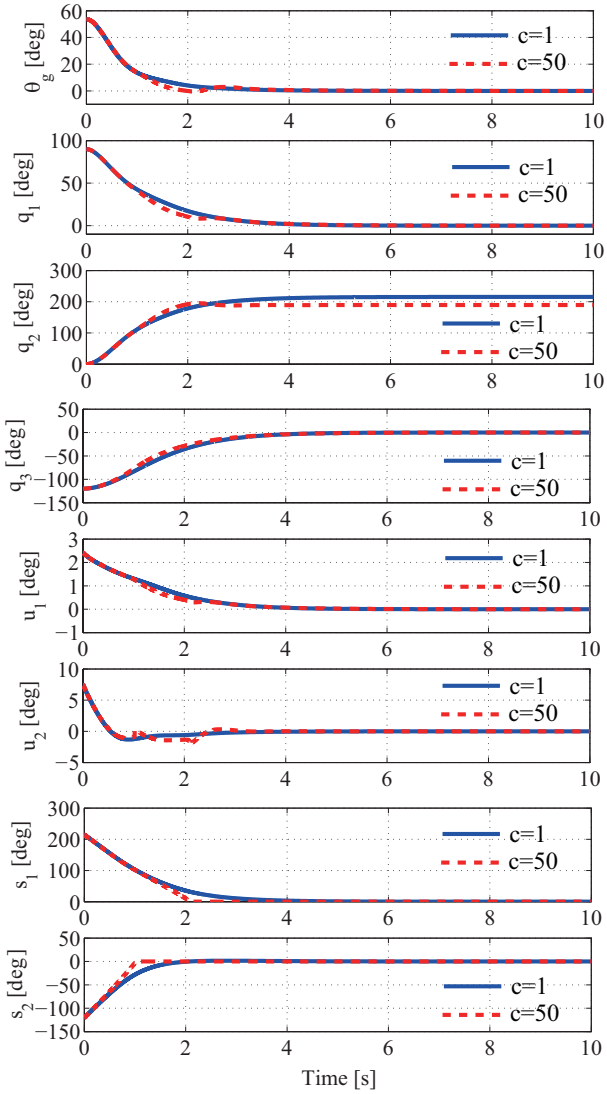

Fig. 5. Time responses of θ_g, q, u and s (simulation).

In order to save the time for the transformation from **1** to **2** in Fig. 2, the initial arm angle $q_3(0)$ is desired to be as close to 0 as possible. However, as $q_3(0)$ becomes closer to 0, a larger torque is required. Thus, similarly to the previous studies [9][10], we set as $q_3(0) = -120$ [deg] in the rest of this section and in the experiment of the next section, taking into account the torque limitation of the real robot.

To prevent chattering, $\mathrm{sgn}(s)$ in (11) is replaced by $\tanh(cs)$, which denotes the vector of the hyperbolic tangent functions of each element of cs where c is a scalar positive design parameter. Fig. 5 shows the time responses of θ_g, q, u and s in the cases of $c = 1$ and $c = 50$. In both cases, q_1 and q_3 are controlled to 0, and q_2 is converging to some constant value, without any problem except that the responses for $c = 50$ are slightly more oscillatory than those for $c = 1$. It can be seen that although the convergence of s_1 and s_2 is slow around 0 for $c = 1$, a significant problem is not found in the responses

of q and θ_g.

VI. Experiment

As in the simulation in Section V, sgn(s) in (11) is replaced by tanh(cs) to prevent chattering in real robot experiments. We choose $c = 1$ based on the simulation results in the previous section. In addition, we need another modification of the control algorithm to apply the proposed method to the real robot. More precisely, the controller is switched from the sliding mode controller (SMC) in (11) to a linear state feedback near the target state, i.e. $[\theta_g, \dot{\theta}_g, \dot{q}_2, q_3, \dot{q}_3] \simeq 0$. The linear state feedback controller has the form $u = -K_{lq}(x - x_r)$, where $x := [q^T, \dot{q}^T]^T$, $x_r := [0, q_2(t_s), 0, 0, 0, 0]$ and t_s is the switching time to the linear controller. The constant matrix K_{lq} is obtained by solving the linear quadratic regulator (LQR) problem [43] for the following linear model

$$\dot{x} = \begin{bmatrix} \dot{q} \\ \bar{A}x + \bar{B}u \end{bmatrix} \tag{27}$$

$$\bar{A} := \frac{\partial \bar{f}}{\partial x}\Big|_{x=x_r} = \frac{\partial \bar{f}}{\partial x}\Big|_{x=0}, \; B := \frac{\partial \bar{g}}{\partial x}\Big|_{x=x_r} = \frac{\partial \bar{g}}{\partial x}\Big|_{x=0} \tag{28}$$

which approximates the original system in (2) near $x = x_r$. The weighting matrices for the state and input in the cost function are chosen as

$$Q_{lq} = \mathrm{diag}\,(5, 8, 3, 5, 1, 1)\,, \qquad R_{lq} = \mathrm{diag}\,(20, 10)$$

respectively. These parameters have been chosen empirically from simulations and experiments with initial states around the target state, since it is difficult to theoretically analyze the stability of the original nonlinear system when the LQR controller is applied.

The switching condition to the linear controller is set as $|\theta_g| < 10$ [deg], $|q_3| < 10$ [deg], $|\dot{q}_2| < 10$ [deg/s]. Note that if the proposed nonlinear controller is used instead of switching to a linear controller around the target state, the robot's position starts moving slowly after the state variables go to the target values. A possible reason for this is that the proposed nonlinear controller does not have a feedback of q_2. More study is needed to incorporate properly the feedback of q_2 into the proposed controller. However, even if this problem is solved, it is possibly better to use a linear controller around the target state, since the parameters of such a linear controller can be customized for the performance around the target state, unlike the proposed nonlinear controller. In order to suppress the effect of the switching, we chose a small constant value of c (=1) in tanh(cs), which makes the control input nearly 0 around the target state. Although we do not focus on other ways to choose c in this paper, there might be more elegant ways. For example, if c is chosen as an increasing function of $|s|$ such that $c = 0$ for $s = 0$, the function tanh(cs) approximates sgn(s) better for large $|s|$ than just choosing a small constant value of c, while it suppresses the effect of switching since c is small around $s = 0$.

Except for this modification, the values of parameters in the control method are same as the ones in Section V. The angle of the main body q_1 is measured by the InertiaCube3 (InterSense Inc.), and the angular velocity $\dot{q}_1$ is measured by a gyro sensor CRS03-04 (Silicon Sensing Systems Japan Ltd.). On the other hand, $\dot{q}_2$ and $\dot{q}_3$ are respectively approximated by the difference quotients of q_2 and q_3, which are measured by rotary encoders. The control input u is computed at every 10 [ms],

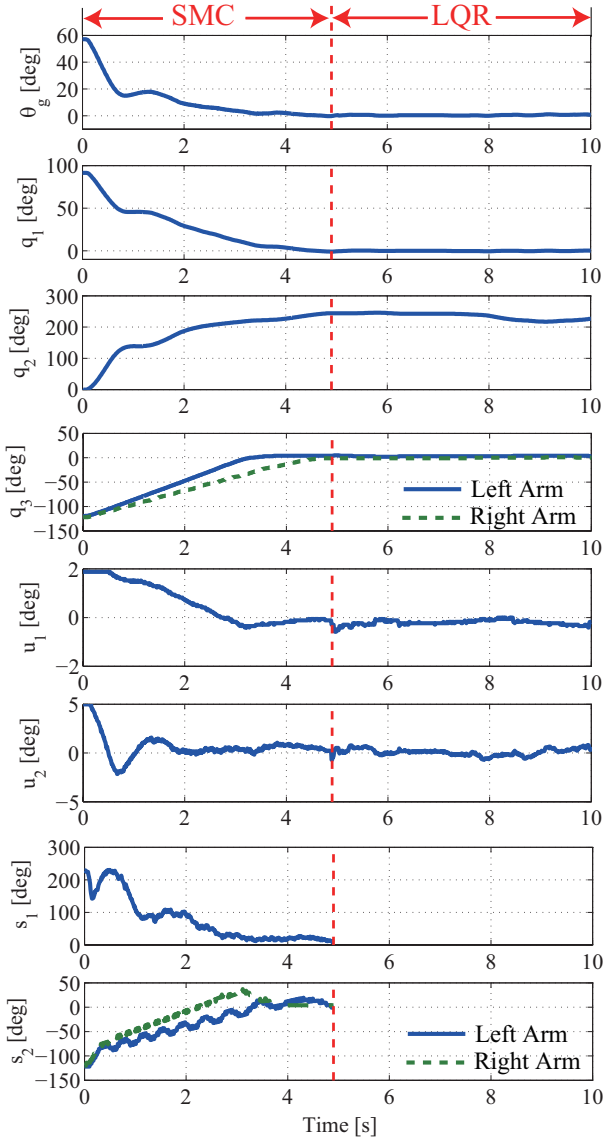

Fig. 6. Time responses of θ_g, q, u and s (experiment).

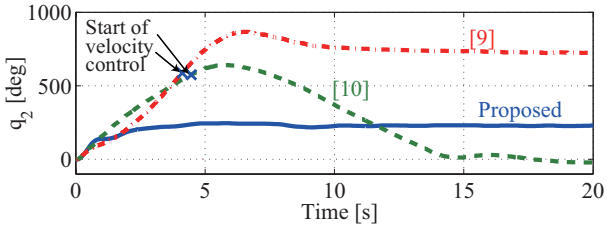

Fig. 7. Comparison of q_2 (experiment).

Fig. 6 shows the time responses of θ_g, q, u and s for the same initial state as the simulation in Fig. 5. The dotted line at $t = 4.9$ [s] illustrates the switching time to the LQR.

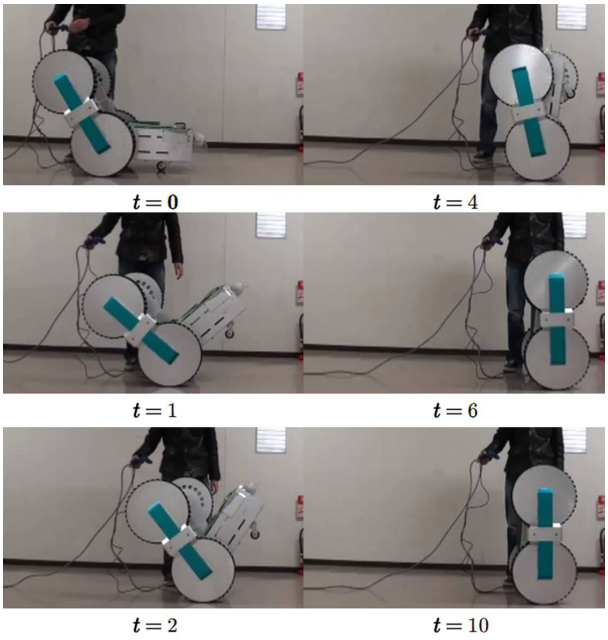

Fig. 8. Snapshot of the experiment.

Note that the responses of s_1 and s_2 are not shown after $t = 4.9$ [s], since the LQR does not use s. A snapshot of the experiment is shown in Fig. 8. These figures show that q_1 and q_3 are controlled to zero and that q_2 is converging to some constant value. Thus, it can be seen that the robot achieved the transformation to the wheeled pendulum and stopped.

Fig. 7 illustrates the comparison of the responses of q_2 by the proposed and conventional methods. As shown in the solid line, the maximum wheel angle during the transformation is $q_2 = 246$ [deg], when the proposed method is used. Since the conventional methods do not control the velocity until θ_g and q_3 become close to 0, they need longer time before $\dot{q}_2$ is controlled to 0. As a result, the maximum wheel angles by the the methods in [9] and [10] are 867 [deg] and 642 [deg] as shown in the dashed and dash-dotted lines, respectively. From the radius of wheels $r = 0.2$ [m], the maximum distance the robot moved from the initial position in the case of the proposed method can be calculated as 0.86 [m], which is significantly smaller than 3.0 [m] in [9] and 2.2 [m] in [10]. This implies that the control method proposed in this paper achieved the transformation in a smaller space than the conventional methods in [9] and [10]. On the other hand, it should be noted that the method in [10] has a merit that the robot position can be controlled as well as the velocity. Thus, the value of q_2 in [10] goes to 0 around $t = 15$.

VII. Conclusions

This paper has presented a sliding mode control method for transformation to an inverted pendulum mode of a mobile robot with wheel-arms. In contrast to the previous transformation methods based on the two-level control, the proposed method can take into account the robot velocity from the beginning of the transformation, which enables to complete the transformation in a smaller space. Furthermore, unlike the previous sliding mode control method for mobile inverted pendulums, the region of attraction on the sliding surface is clarified by deriving an invariant set in which the system state converges to the origin without going out. The effectiveness of the proposed method has been demonstrated in both simulations and real robot experiments. The robot in this paper has the same form with ordinary inverted pendulum type wheeled robots, when the arm angles are fixed to zero. Therefore, the proposed nonlinear control method is expected to be effective for other vehicles of inverted pendulum type, especially in situations where the state of such a vehicle is away from the equilibrium point. Possible future works are the stability analysis off the sliding surface and the control design taking into account the modeling error and motor torque limits.

Appendix

Proof of Theorem 1

We use the following fact to prove Theorem 1.

Lemma 1: Under Assumption 1, we have

$$\underline{F}_1 \le F_1 \le \bar{F}_1, \quad \underline{F}_2 \le F_2. \tag{29}$$

Proof: We first show the inequalities for F_1. Note that $F_1(\theta_g)$ is an even function, i.e. $F_1(\theta_g) = F_1(-\theta_g)$. Thus, it suffices to consider the case of $0 \le \theta_g \le \pi/2$, since the possible range of θ_g is $|\theta_g| \le \pi/2$. From $d_2 > 0$ in (23) and

$$\frac{\partial F_1}{\partial \theta_g} = \frac{(a_1 d_2 - a_2 d_1)\sin\theta_g}{(d_1 + d_2\cos\theta_g)^2}, \tag{30}$$

it can be seen that

$$\frac{\partial F_1}{\partial \theta_g} \ge 0, \quad \text{if} \quad a_1 d_2 \ge a_2 d_1 \tag{31}$$

$$\frac{\partial F_1}{\partial \theta_g} < 0, \quad \text{if} \quad a_1 d_2 < a_2 d_1 \tag{32}$$

for $\theta_g > 0$ and that $\frac{\partial F_1}{\partial \theta_g} = 0$ for $\theta_g = 0$. Therefore, there are only three cases where $F_1(\theta_g)$ is (i) monotonically increasing, (ii) monotonically decreasing, and (iii) constant, for $0 \le \theta_g \le \pi/2$. In each case, the maximum and minimum of $F_1(\theta_g)$ are $F_1(0)$ or $F_1(\pi/2)$, which concludes the proof of the inequalities for F_1.

We next show the inequality for F_2. From the assumption in (23), we have $d_1 > 0$ and $d_2 > 0$. Thus, since $b_1 > 0$ and $b_2 > 0$, we obtain $\underline{F}_2 \le F_2$ for $|\theta_g| \le \pi/2$. ■

By differentiating V, we obtain

$$\dot{V} = 2\{p_{11}\theta_g\dot{\theta}_g + p_{12}(\dot{\theta}_g^2 + \theta_g\ddot{\theta}_g) + p_{22}\dot{\theta}_g\ddot{\theta}_g\}. \tag{33}$$

Then, by substituting (18) into (33), we have

$$\begin{aligned}\dot{V} = &-2(p_{12}F_1 + p_{22}F_2\xi - p_{11})\theta_g\dot{\theta}_g \\ &-2(p_{22}F_1 - p_{12})\dot{\theta}_g^2 - 2p_{12}F_2\xi\theta_g^2\end{aligned} \tag{34}$$

where $\xi := \frac{\sin\theta_g}{\theta_g}$. Eq. (34) is rewritten as

$$\begin{aligned}\dot{V} = &-2p_{12}F_2\xi\left(\theta_g + \frac{p_{12}F_1 + p_{22}F_2\xi - p_{11}}{2p_{12}F_2\xi}\dot{\theta}_g\right)^2 \\ &+ 2\left\{\frac{(p_{12}F_1 + p_{22}F_2\xi - p_{11})^2}{4p_{12}F_2\xi} + p_{12} - p_{22}F_1\right\}\dot{\theta}_g^2\end{aligned} \tag{35}$$

by completing the square with respect to θ_g. From $d_1 > 0$, $d_2 > 0$, $b_1 > 0$, $b_2 > 0$ and $|\theta_g| \leq \frac{\pi}{2}$, we have $F_2 > 0$ and $\xi > 0$, which imply $p_{12}F_2\xi > 0$ under the assumption that $p_{12} > 0$ in (24). Thus, (35) implies that a sufficient condition for $\dot{V} < 0$ is

$$(p_{12}F_1 + p_{22}F_2\xi - p_{11})^2 + 4p_{12}F_2\xi(p_{12} - p_{22}F_1) < 0$$

which can be rewritten as

$$\begin{aligned} &p_{22}^2(\xi F_2 - h_1)^2 - h_2 < 0 \qquad (36)\\ &h_1 := \frac{p_{22}(p_{12}F_1 + p_{11}) - 2p_{12}^2}{p_{22}^2}\\ &h_2 := p_{22}^2 h_1^2 - (p_{12}F_1 - p_{11})^2 \end{aligned}$$

by completing the square with respect to F_2. From the assumption in (24) and $\underline{F}_1 \leq F_1 \leq \bar{F}_1$, we have

$$0 < p_{11} - p_{12}\bar{F}_1 \leq p_{11} - p_{12}F_1 \leq p_{11} - p_{12}\underline{F}_1 \qquad (37)$$

which implies $h_2 \geq \underline{h}_2$. Thus, we have $h_2 > 0$ from the assumption that $\underline{h}_2 > 0$ in (23). Therefore, the condition in (36) is written as

$$-\sqrt{h_2} < p_{22}(\xi F_2 - h_1) < \sqrt{h_2}. \qquad (38)$$

We now show that the inequality on the left in (38) is satisfied for each x_θ which satisfies $|\theta_g| \leq \pi/2$. It holds from Lemma 1 that $F_2 \geq \underline{F}_2 > 0$. From $\underline{F}_1 \leq F_1 \leq \bar{F}_1$ in Lemma 1, $p_{12} > 0$ in (24), and $p_{22} > 0$ due to the positive definiteness of P, we have $\underline{h}_1 \leq h_1 \leq \bar{h}_1$. Thus, it holds from $\xi = \sin\theta_g/\theta_g \geq 2/\pi$ and $\underline{h}_1 > 0$ in (23) that

$$p_{22}(\xi F_2 - h_1) + \sqrt{h_2} \geq p_{22}(\frac{2}{\pi}\underline{F}_2 - \bar{h}_1) + \sqrt{\underline{h}_2}.$$

Therefore, it can be shown from the assumption in (25) that the inequality on the left in (38) is satisfied. This implies that the inequality on the right in (38) is a sufficient condition for $\dot{V} < 0$.

We next derive a sufficient condition for the inequality on the right in (38) to be satisfied. Since $\xi \leq 1$ for $|\theta_g| \leq \pi/2$, a sufficient condition for the inequality on the right in (38) is

$$p_{22}(F_2 - \underline{h}_1) < \sqrt{\underline{h}_2},$$

which implies

$$\frac{b_1 + b_2\dot{\theta}_g^2}{d_1 + d_2\cos\theta_g} < S \qquad (39)$$

from the definitions of F_2 and S. Thus,

$$b_2\dot{\theta}_g^2 - Sd_2\cos\theta_g < Sd_1 - b_1 \qquad (40)$$

since $d_1 + d_2\cos\theta_g > 0$ from (23) and $|\theta_g| \leq \pi/2$. By substituting $\sin^2\frac{\theta_g}{2} = \frac{1-\cos\theta_g}{2}$ into (40), we obtain

$$b_2\dot{\theta}_g^2 + Sd_2\left(2\sin^2\frac{\theta_g}{2} - 1\right) < Sd_1 - b_1. \qquad (41)$$

Further, since $|\sin(\theta_g/2)| \leq \theta_g/2$ for $|\theta_g| \leq \pi/2$, a sufficient condition for (41) is

$$b_2\dot{\theta}_g^2 + Sd_2\left(\frac{\theta_g^2}{2} - 1\right) < Sd_1 - b_1.$$

This implies from the assumption in (26) that

$$\frac{Sd_2}{2\{S(d_1+d_2) - b_1\}}\theta_g^2 + \frac{b_2}{S(d_1+d_2) - b_1}\dot{\theta}_g^2 < 1. \qquad (42)$$

Therefore, it can be seen from the definitions of U that

$$x_\theta^T U x_\theta < 1 \qquad (43)$$

is a sufficient condition for the inequality on the right in (38) to be satisfied. This implies that (43) is a sufficient condition for $\dot{V} < 0$.

We finally show that $\mathcal{E}$ is included in the ellipsoid described in (43). To this end, we define $y := \gamma^{-\frac{1}{2}}P^{\frac{1}{2}}x_\theta$ and substitute $x_\theta = \gamma^{\frac{1}{2}}P^{-\frac{1}{2}}y$ into the left hand side in (43) to obtain

$$x_\theta^T U x_\theta = \gamma y^T P^{-\frac{1}{2}} U P^{-\frac{1}{2}} y = \gamma\|U^{\frac{1}{2}}P^{-\frac{1}{2}}y\|^2. \qquad (44)$$

In $\mathcal{E}$, it holds that $\gamma^{-1}x_\theta^T P x_\theta < 1$, which implies $\|y\| < 1$. Thus, we have

$$\|U^{\frac{1}{2}}P^{-\frac{1}{2}}y\|^2 < \|U^{\frac{1}{2}}P^{-\frac{1}{2}}\|^2 = 1/\gamma, \qquad (45)$$

since $\|U^{\frac{1}{2}}P^{-\frac{1}{2}}\|$ is the maximum singular value of $U^{\frac{1}{2}}P^{-\frac{1}{2}}$, which is equivalent to the square root of the maximum eigenvalue of $P^{-\frac{1}{2}}UP^{-\frac{1}{2}}$. Therefore, (43) is satisfied from (44) and (45).

REFERENCES

[1] Y. Spector, D. Raz, A. Novoplanski, and G. Rinberg, "Adaptable traction system of a vechile," US published patent application, 2008-0061627-2008.

[2] O. Matsumoto, S. Kajita, M. Saigo and K. Tani, "Dynamic trajectory control of passing over stairs by a biped type leg-wheeled robot with nominal reference of static gait," in *Proc. IEEE/RSJ Int. Conf. Intell. Robots and Syst.*, pp. 406-412, 1998.

[3] O. Matsumoto, S. Kajita and K. Komoriya, "Flexible locomotion control of a self-contained biped leg-wheeled system," in *Proc. IEEE/RSJ Int. Conf. Intell. Robots and Syst.*, pp. 2599-2604, 2002.

[4] M. Lauria, Y. Piguet and R. Siegwart, "Octopus - an autonomous wheeled climbing robot," in *Proc. the Fifth International Conference on Climbing and Walking Robots*, 2002.

[5] T. Estier, Y. Crausaz, B. Merminod, M. Lauria, R. Piguet, R. Siegwart, "An innovative Space Rover with Extended Climbing Alilities," in *Proc. Space and Robotics*, 2000.

[6] C. Grand, F. Benamar, F. Plumet, and P. Bidaud, "Stability and traction optimization of a reconfigurable wheel-legged robot," *Int. J. Robot. Res*, vol.23, no.10-11, pp.1041-1058, 2004.

[7] N. Shiroma, Y. Chiu, Z. Min, I. Kawabuchi, and F. Matsuno, "Development and control of a high maneuverability wheeled robot with variable-structure functionality," in *Proc. IEEE/RSJ Int. Conf. Intell. Robots and Syst.*, pp. 4001-4006, 2006.

[8] N. Shiroma, Y. Fujino, and F. Mstauno, "Automatic step climbing by wheeled robot HANZO with variable structure functionality using 3D range sensor," in *Proc. IEEE Int. Workshop on Safety, Security and Rescue Robotics*, 2006.

[9] H. Fukushima, S. Shinmura, and F. Matsuno, "Transformation control to an inverted pendulum mode of a mobile robot with wheel-arms using partial linearization," in *Proc. IEEE Int. Conf. Robot. and Autom.*, pp. 1683–1688, 2011.

[10] H. Fukushima, M. Kakue, K. Kon and F. Matsuno, "Transformation control to an inverted pendulum for a mobile robot with wheel-arms using partial linearization and polytopic model set," *IEEE Trans. Robot.*, vol.29, no.3, pp.774-783, 2013.

[11] Y.-S. Ha and S. Yuta, "Trajectory tracking control for navigation of the inverse pendulum type self-contained mobile robot," *Robot. Autonom. Syst.*, vol. 17, pp. 65-80, 1996.

[12] F. Grasser, A. D'Arrigo, S. Colombi, and A. Rufer, "Joe: A mobile, inverted pendulum," *IEEE Trans. Ind. Electron.*, vol. 49, no. 1, pp. 107-114, 2002.

[13] A. Blankespoor and R. Roemer, "Experimental verification of the dynamic model for a quarter size self-balancing wheelchair," in *Proc. Amer. Contr. Conf.*, pp. 488-492, 2004.
[14] Y. Kim, S. H. Kim, and Y. K. Kwak, "Dynamic analysis of a nonholonomic two-wheeled inverted pendulum robot," *J. Intell. Robot. Syst.*, vol. 44, no. 1, pp. 25–46, 2005.
[15] T. J. Ren, T. C. Chen, and C. J. Chen, "Motion control for a two-wheeled vehicle using a self-tuning PID controller," *Control Eng. Practice*, vol. 16, no. 3, pp. 365–375, 2008.
[16] A. Salerno and J. Angeles, "The control of semi-autonomous two-wheeled robots undergoing large payload-variations," in *Proc. IEEE Int. Conf. Robot. Autom.*, pp. 1740-1745, 2004.
[17] K. Pathak, J. Franch, and S. K. Agrawal, "Velocity and position control of a wheeled inverted pendulum by partial feedback linearization," *IEEE Trans. Robot.*, vol.21, no.3, pp.505-513, 2005.
[18] K. Pathak and S. Agrawal, "Band-limited trajectory planning and tracking for certain dynamically stabilized mobile systems," *Trans. ASME, Journal of Dynamic Systems, Measurement and Control*, vol.128, pp.104-111, 2006.
[19] D. S. Nasrallah, H. Michalska, and J. Angeles, "Controllability and posture control of a wheeled pendulum moving on an inclined plane," *IEEE Trans. Robot.*, vol.23, no.3, pp.564-577, 2007.
[20] M. T. Ravichandran, and A. D. Mahindrakar, "Robust stabilization of a class of underactuated mechanical systems using time scaling and Lyapunov redesign," *IEEE Trans. Ind. Electron.*, vol.58, no.9, pp.4299-4313, 2011.
[21] C.-H. Chiu, Y.-W. Lin, and C.-H. Lin, "Real-time control of a wheeled inverted pendulum based on an intelligent model free controller," *Mechatronics*, vol.21, pp.523-533, 2011.
[22] C.-H. Chiu, Y.-F. Peng, and Y.-W. Lin, "Robust intelligent backstepping tracking control for wheeled inverted pendulum," *Soft Comput.*, vol.15, pp.2029-2040, 2011.
[23] C. Yang, Z. Li, and J. Li, "Trajectory planning and optimized adaptive control for a class of wheeled inverted pendulum vehicle models," *IEEE Trans. Cybernetics*, vol.43, no.1, pp.24-36, 2013.
[24] J. M. Maciejowski, *Predictive control with constraints*. Harlow, U.K.: Prentice-Hall, 2002.
[25] D. Q. Mayne, J. B. Rawlings, C. V. Rao, and P. O. Scokaert, "Constrained model predictive control: Stability and optimality," *Automatica*, 36, pp. 789–814, 2000.
[26] H. Fukushima and R. R. Bitmead, "Robust constrained predictive control using comparison model," *Automatica*, vol. 41, no. 1, pp. 97–106, 2005.
[27] Z. Li, and J. Luo, "Adaptive robust dynamic balance and motion controls of mobile wheeled inverted pendulums," *IEEE Trans. Contr. Syst. Technol.*, vol.17, no.1, pp.233-241, 2009.
[28] Z. Li, and J. Luo, "Adaptive motion/force control of mobile underactuated manipulators with dynamics uncertainties by dynamic coupling and output feedback," *IEEE Trans. Contr. Syst. Technol.*, vol.18, no.5, pp.1068-1079, 2010.
[29] Z. Li, Y. Zhang, and Y. Yang, "Support vector machine optimal control for mobile wheeled inverted pendulums with unmodelled dynamics," *Neurocomputing*, vol.73, pp. 2773–2782, 2010.
[30] Z. Li, and C. Yang, "Neural-adaptive output feedback control of a class of transportation vehicles based on wheeled inverted pendulum models," *IEEE Trans. Contr. Syst. Technol.*, vol.20, no.6, pp.1583-1591, 2012.
[31] J. Huang, Z.-H. Guan, T. Matsuno, T. Fukuda, and K. Sekiyama, "Sliding-mode velocity control of mobile-wheeled Inverted-Pendulum Systems," *IEEE Trans. Robot.*, vol. 26, no. 4, pp. 750-758, 2010.
[32] J.-X. Xu, Z.-Q. Guo, and T. H. Lee, "Design and implementation of integral sliding-mode control on an underactuated two-wheeled mobile robot," *IEEE Trans. Ind. Electron.*, vol.61, no.7, pp.3671-3681, 2014.
[33] J.-X. Xua, Z.-Q. Guo, and T. H. Lee, "Synthesized design of a fuzzy logic controller for an underactuated unicycle," *Fuzzy Sets and Systems*, vol.207, pp. 77–93, 2012.
[34] C.-H. Huang, W.-J. Wang, and C.-H. Chiu, "Design and implementation of fuzzy control on a two-wheel inverted pendulum," *IEEE Trans. Ind. Electron.*, vol.58, no.7, pp.2988-3001, 2011.
[35] C.-H. Chiu and C.-C. Chang, "Design and development of Mamdani-like fuzzy control algorithm for a wheeled human-conveyance vehicle control," *IEEE Trans. Ind. Electron.*, vol.59, no.12, pp.4774-4783, 2012.
[36] J.-X. Xu, Z.-Q. Guo, and T. H. Lee, "Design and Implementation of a Takagi-Sugeno-type fuzzy logic controller on a two-wheeled mobile robot," *IEEE Trans. Ind. Electron.*, vol.60, no.12, pp.5717-5728, 2013.
[37] S. Jung, and S. S. Kim, "Control experiment of a wheel-driven mobile inverted pendulum using neural network," *IEEE Trans. Contr. Syst. Technol.*, vol.16, no.2, pp.297-303, 2008.
[38] S.-H. Jeong and T. Takahashi, "Stable and quick standing-sitting motion of I-PENTAR by whole-body motion with force control," in *Proc. IEEE/RSJ Int. Conf. Intell. Robots Syst.*, pp. 199–204, 2008.
[39] T. Yasui and K. Yamafuji, "Motion control of the parallel bicycle-type mobile robot which is composed of a triple inverted pendulum : 1st report, stability control of standing upright, ascending and descending of stairs," *Trans. JSME*, vol. C-57, no. 538, pp. 1904–1909, 1991. (in Japanese)
[40] K. Yamafuji, M. Q. Feng, and T. Kawamura, "Robot driven by parallel bicycles," *Int. J. Mechanics and Control*, vol. 9, no. 2, pp. 3–10, 2008.
[41] J.-J. Slotineand W. Li, *Applied Nonlinear Control*. Englewood Cliffs, NJ: Prentice-Hall, 1991.
[42] J.-J. Wang, "Stabilization and tracking control of $X - Z$ inverted pendulum with sliding-mode control," *ISA Transactions*, vol. 51, no. 6, pp. 763–770, 2012.
[43] B. D. O. Anderson and J. B. Moore, *Optimal Control: Linear Quadratic Methods*. Englewood Cliffs, NJ: Prentice-Hall, 1990.

Hiroaki Fukushima (M'06) received the B.S. and M.S. degrees in engineering and Ph.D. degree in informatics from Kyoto University, Japan, in 1995, 1998 and 2001, respectively. From 1999 to 2004 he was a Research Fellow of Japan Society for the Promotion of Science. From 2004 to 2009 he worked as a Research Associate and Assistant Professor at the University of Electro-Communications, Japan. Currently he is an Assistant Professor of Kyoto University, Japan. His research interests include system identification and robust control. He is a member of the IEEE, SICE, ISCIE and RSJ.

Keiji Muro received the B.S. degree in engineering from Kyoto University, Japan, in 2013. He is currently a graduate student at Kyoto University. His research interests include motion control of mobile robots and nonlinear control theory.

Fumitoshi Matsuno (M'94) received the PhD (Dr. Eng.) degree from Osaka University in 1986. In 1986 he joined the Department of Control Engineering, Osaka University. Since 2009, he has been a Professor in the Department of Mechanical Engineering and Science, Kyoto University. He holds also a post of the Vice-President of NPO International Rescue System Institute (IRS). His current research interests lie in robotics, swarm intelligence, control of distributed parameter system and nonlinear system, and rescue support system in disaster. Dr. Matsuno received many awards including the Outstanding Paper Award in 2001 and 2006, Takeda Memorial Prize in 2001 from the Society of Instrument and Control Engineers (SICE), and the Best Paper Award in 2013 from Information Processing Society of Japan. He is a Fellow member of the SICE, the JSME, and a member of the IEEE, the RSJ, the ISCIE, among other organizations.